JGR Space Physics

RESEARCH ARTICLE
10.1029/2021JA030177

Special Section:
SOUTHTRAC-GW: An airborne field campaign to explore gravity wave dynamics at the world's strongest hotspot

Mesosphere and Lower Thermosphere Winds and Tidal Variations During the 2019 Antarctic Sudden Stratospheric Warming

Guiping Liu[1,2], Diego Janches[3], Jun Ma[4], Ruth S. Lieberman[3], Gunter Stober[5], Tracy Moffat-Griffin[6], Nicholas J. Mitchell[6,7], Jeong-Han Kim[8], Changsup Lee[8], and Damian J. Murphy[9]

[1]Space Sciences Laboratory, University of California, Berkeley, CA, USA, [2]CUA/NASA GSFC, Greenbelt, MD, USA, [3]Heliophysics Science Division, NASA Goddard Space Flight Center, Greenbelt, MD, USA, [4]Space Sciences Division, Naval Research Laboratory, Washington, DC, USA, [5]Institute of Applied Physics & Oeschger Center for Climate Change Research, Microwave Physics, University of Bern, Bern, Switzerland, [6]British Antarctic Survey, Cambridge, UK, [7]Centre for Space, Atmospheric and Oceanic Science, University of Bath, Claverton Down, Bath, UK, [8]Division of Atmospheric Sciences, Korea Polar Research Institute, Incheon, South Korea, [9]Australian Antarctic Division, Kingston, Tasmania, Australia

Key Points:

- High-altitude meteorological analysis results with data assimilation are consistent with the meteor radar measurements near 60°S latitude
- Day-to-day variations in the zonal and meridional winds at ~80–90 km altitude are captured by the analysis system
- Both analyzed and observed winds reveal a large tidal variation at ~90 km altitude during the 2019 Antarctic stratospheric warming

Correspondence to:
G. Liu,
guiping@berkeley.edu

Citation:
Liu, G., Janches, D., Ma, J., Lieberman, R. S., Stober, G., Moffat-Griffin, T., et al. (2022). Mesosphere and lower thermosphere winds and tidal variations during the 2019 Antarctic Sudden Stratospheric Warming. *Journal of Geophysical Research: Space Physics*, *127*, e2021JA030177. https://doi.org/10.1029/2021JA030177

Received 2 DEC 2021
Accepted 28 FEB 2022

Abstract Realistic modeling of the winds and dynamical variations in the mesosphere and lower thermosphere (MLT) at Southern Hemisphere (SH) mid-to-high latitudes near 60°S where dramatic motions occur has been a challenge. This work presents an evaluation of the MLT zonal and meridional winds from ~80 to 98 km altitude produced by the high-altitude version of the Navy Global Environmental Model (NAVGEM-HA) numerical weather prediction system during the Antarctic Sudden Stratospheric Warming (SSW) in September 2019. These results are compared with the coincident measurements by five meteor radars at Tierra del Fuego (TDF; 53.7°S, 67.7°W), King Edward Point (KEP; 54.3°S, 36.5°W), King Sejong Station (KSS; 62.2°S, 58.8°W), Rothera (ROT; 67.5°S, 68.0°W), and Davis (DAV; 68.6°S, 78.0°E) across SH mid-to-high latitudes. We find that the day-to-day variations in NAVGEM-HA winds related to tidal motions are overall consistent with variations in the radar winds, and the daily mean winds have a correlation of 0.7–0.9 between them. Three-hourly NAVGEM-HA winds have a correlation of ~0.5 and mean difference <10 m/s to the radar observations at most stations, and the Root Mean Square (RMS) error ranges from ~25 to 35 m/s. Above 90 km altitude, the correlation coefficient decreases, and the difference and RMS error increase, indicating an upper limit to the validity of the NAVGEM-HA results. Both the analyzed and observed winds reveal an enhancement in diurnal and semidiurnal tidal amplitude during this SH SSW. NAVGEM-HA shows some evidence that nonmigrating tidal enhancements are produced through the interaction of migrating tides with planetary waves.

Plain Language Summary High Altitude (HA) meteorological analysis products of the Navy Global Environmental Model (NAVGEM) that assimilates various observations are believed to be able to provide a realistic description of the state of the mesosphere and lower thermosphere (MLT). Dramatic motions of the MLT region are detected during austral winter in the Southern Hemisphere (SH) over the area extending from the Southern Andes to the Drake Passage and the Antarctic Peninsula. Yet, due to lack of global wind observations, this dynamically active region has not been well explored. Sudden Stratospheric Warmings (SSWs) are manifestations of dynamic disruptions in the winter polar area, and in September 2019 an unusual SSW occurred over Antarctica. This study evaluates the evolution of MLT winds and related tidal variations during this SSW, using both the NAVGEM-HA analysis results and the meteor radar observations at several locations within this very dynamic region. We have performed a one-to-one comparison and found that the analyzed daily mean winds generally agree with the observations. The NAVGEM-HA numerical forecast system also captures the enhanced tidal motions observed by the radars during this Antarctic SSW.

1. Introduction

The mesosphere and lower thermosphere (MLT) exhibit dramatic variations during austral winter near 60° latitude in the Southern Hemisphere (SH), covering the Southern Andes, the Drake Passage, and the Antarctic Peninsula area (e.g., Alexander et al., 2008; de Wit et al., 2017; Dowdy et al., 2004; Fritts et al., 2019; Liu, Janches, et al., 2021; Stober, Baumgarten, et al., 2020; Stober, Janches, et al., 2020). These variations account for both

large- and small-scale motions including tides and gravity waves. Semidiurnal tides are prominent at these latitudes, achieving maximum amplitudes between 50° and 70°S, whereas diurnal tides dominate at lower latitudes (e.g., Hagan et al., 1999; Hagan & Forbes, 2003). Gravity wave variances and momentum fluxes also maximize in this region (Alexander et al., 2008; Ern et al., 2004; Wu & Eckermann, 2008). Enhanced gravity wave activities have been related to the perturbations of tropospheric winds by high mountains (e.g., Eckermann et al., 2006; Hertzog et al., 2008; Jiang et al., 2002), and the jet-front system could also play a significant role (e.g., Guest et al., 2000). However, this very dynamic region at SH mid-to-high latitudes is still poorly understood and needs to be further explored.

There are very sparse observations of the MLT winds near 60°S latitude, and thus our understanding of dynamics within this highly active region is limited. Available observations are mostly obtained from ground-based medium frequency and meteor radars. These observations have continuous temporal sampling, but their spatial coverage is limited to only certain geographic locations (e.g., Stober, Janches, et al., 2020; Stober, Baumgarten, et al., 2020). Global winds have been simulated using general circulation models, but the modeled winds exhibit substantial discrepancies among different models (e.g., McCormack et al., 2021; Pedatella et al., 2014). Parameterizations of gravity waves in whole atmosphere models are normally not sufficient (Garcia et al., 2017), and simulations of the breaking of very strong mountain waves over the Southern Andes and the Antarctic Peninsula are not adequate (e.g., Becker & Vadas, 2018). Understanding the SH mid-to-high latitude MLT region has therefore remained challenging.

To address this need for improved description of global MLT dynamics, a high-altitude version of the Navy Global Environmental Model (or NAVGEM-HA) has been developed for MLT research (Eckermann et al., 2018; Hoppel et al., 2013; McCormack et al., 2017, 2021). NAVGEM-HA is a numerical weather prediction system that combines a global spectral forecast model with an advanced data assimilation system to produce global synoptic meteorological products extending from the surface to approximately 100 km altitude. Earlier studies have shown that NAVGEM-HA provides a good representation of the MLT winds for two boreal winters in 2009–2010 and 2012–2013 (Eckermann et al., 2018; McCormack et al., 2017). Direct comparisons of these analysis results to the meteor radar measurements have also been performed for the seasonal mean winds involving three radars in the Northern Hemisphere (NH; Stober, Baumgarten et al., 2020). Here this study extends such a direct comparison to include five radar stations across SH mid-to-high latitudes, and the study focuses on the day-to-day variations during a rare Antarctic Sudden Stratospheric Warming (SSW) in September 2019. Large disturbances in the MLT winds have been observed during this SSW (e.g., Liu, Janches, et al., 2021; Stober, Janches, et al., 2020). This study further assesses the NAVGEM-HA results and investigates the MLT tidal variations in response to the SH SSW.

SSWs are driven by vertically propagating planetary waves that are generated in the troposphere by land-sea heating contrast and orography (e.g., Matsuno, 1971). Although SSWs are predominantly a stratospheric phenomenon, there are related impacts occurring throughout the mesosphere, thermosphere and ionosphere (e.g., Chau et al., 2012; Goncharenko et al., 2021; Liu & Roble, 2002; Oberheide et al., 2020; Pedatella et al., 2018; Pedatella & Forbes, 2010; Shepherd et al., 2014; Yamazaki et al., 2020). Planetary waves dominate in the polar region, and they can modify tides at a wide range of latitudes and extend their influences into the MLT (e.g., Lieberman et al., 2015, 2004; Liu et al., 2010; Pancheva et al., 2009; Pedatella & Forbes, 2010). Indeed, tidal responses to SSWs have been reported using both observations and simulations (e.g., Fuller-Rowell et al., 2010; Hibbins et al., 2019; Lieberman et al., 2015; Liu, Lieberman, et al., 2021; Pedatella et al., 2012). Some tides dissipate in the MLT region due to eddy and molecular diffusion, and dissipating tides deposit their momentum and energy into the mean flow, modifying the large-scale circulation (e.g., Forbes et al., 2008). Tides with long vertical wavelengths are able to propagate upward to the lower thermosphere, where they modify the wind-driven dynamo electric fields and cause the longitudinal structures in the ionosphere (e.g., England et al., 2006; Forbes et al., 2008; Pedatella & Liu, 2013). SSWs have been recognized as a driver of the upper atmosphere variability (e.g., Goncharenko et al., 2021).

In this study, we examine the NAVGEM-HA zonal and meridional wind fields for August and September of 2019, spanning the entire Antarctic SSW event. The goal is to examine the dynamical evolution of the MLT region before, during, and after this unusual SH SSW. Specifically, we aim to determine the tidal response to the 2019 SSW in NAVGEM-HA MLT winds at mid-to-high latitudes in the SH. We have performed a one-to-one comparison of the NAVGEM-HA results with the coincident measurements by five meteor radars, showing that both the

Table 1
Locations of the Meteor Radars Used for This Study

Station	Location (latitude, longitude)
Tierra del Fuego (TDF)	53.7°S, 67.7°W
King Edward Point (KEP)	54.3°S, 36.5°W
King Sejong Station (KSS)	62.2°S, 58.8°W
Rothera (ROT)	67.5°S, 68.0°W
Davis (DAV)	68.6°S, 78.0°E

MLT winds and tides from NAVGEM-HA agree with the observations for most stations at ~80–90 km altitude, but for some stations and higher altitudes there are noticeable differences. This study demonstrates that although more work is needed, the NAVGEM-HA system is able to realistically define the winds and tidal variations in the MLT region near 60°S during the 2019 SH SSW.

2. Data and Analysis Methods

2.1. NAVGEM-HA Analysis

NAVGEM-HA is an extension of the Navy operational weather forecast system (Hogan et al., 2014) up to the level at 6×10^{-5} hPa (~116 km altitude) and the vertical spacing is ~2 km in the stratosphere and the mesosphere (McCormack et al., 2017, 2021). The top levels of the system at above ~100 km altitude are specified with strong diffusion in order to reduce the wave reflection. Thus, only analysis results below ~100 km are valid. The NAVGEM-HA has provided a global description of atmospheric wind, temperature and composition from the surface to ~100 km.

A data assimilation algorithm has been implemented in NAVGEM-HA to assimilate various in-situ and remote sensing observations, including those from surface reports, radiosondes, ship, aircraft, and satellites. The system also assimilates temperature, ozone mixing ratio, and water vapor mixing ratio profiles from the Microwave Limb Sounder (MLS) on the Aura satellite, temperature profiles from the Sounding of the Atmosphere using Broadband Emission of Radiation (SABER) instrument on the Thermosphere Ionosphere Mesosphere Energetics and Dynamics (TIMED) satellite, and microwave radiances from the Upper Atmosphere Sounding (UAS) channels of the Special Sensor Microwave Imager/Sounder (SSMIS) on the F17 Defense Meteorological Satellite Program (DMSP). The assimilation is performed every 6 hr, and by including the 3-hourly forecast output of atmospheric variables, global wind fields are generated every 3 hr on 1° latitude and longitude grids. The assimilation of combined MLS, SABER, and SSMIS/UAS data is unique to NAVGEM-HA, and these observations provide valuable information on the state of the MLT region needed to capture the large-scale response to the SSW.

2.2. Meteor Radar Winds

Table 1 lists the five meteor radars used for this study. These are located at Tierra del Feugo (TDF; 53.7°S, 67.7°W) in Southern Argentina, King Edward Point (KEP; 54.3°S, 36.5°W) on South Georgia Island, King Sejong Station (KSS; 62.2°S, 58.8°W) on King George Island, Rothera (ROT; 67.5°S, 68.0°W) on the Antarctic Peninsula, and Davis (DAV; 68.6°S, 78.0°E) on the other side of the Antarctic continent approximately opposite Rothera (see Figure 1). All of these radars employ the all-sky interferometer to measure the MLT winds at high resolutions (e.g., Fritts, Janches, & Hocking, 2010; Fritts, Janches, Iimura, et al., 2010; Holdsworth et al., 2008; Kim et al., 2010; Lee et al., 2013; Sandford et al., 2010). Using meteor trails, hourly zonal and meridional winds are derived at ~2–3 km altitude bins in the altitude range from ~80 to 100 km. Meteors are mainly detected across this range, and the meteor distribution follows a Gaussian pattern with the maximum count of ~several hundreds of meteors peaking at ~90 km (e.g., Fritts, Janches, & Hocking, 2010; Fritts, Janches, Iimura, et al., 2010). Winds are calculated only when sufficient meteors are recorded at one bin. The winds derived have the uncertainties of ~2 m/s at ~90 km, and the uncertainties increase at lower and higher levels reaching the largest values of ~12 m/s at the bottom and top bins. The meteor radar wind data have been shown to be valuable for quantifying the dynamical variations in the MLT region, including small-scale gravity wave momentum fluxes (e.g., de Wit et al., 2017). Except for occasional data gaps, the wind data are almost continuously available at all stations throughout the 2019 Antarctic SSW. These available data are adequate to compare with the NAVGEM-HA winds.

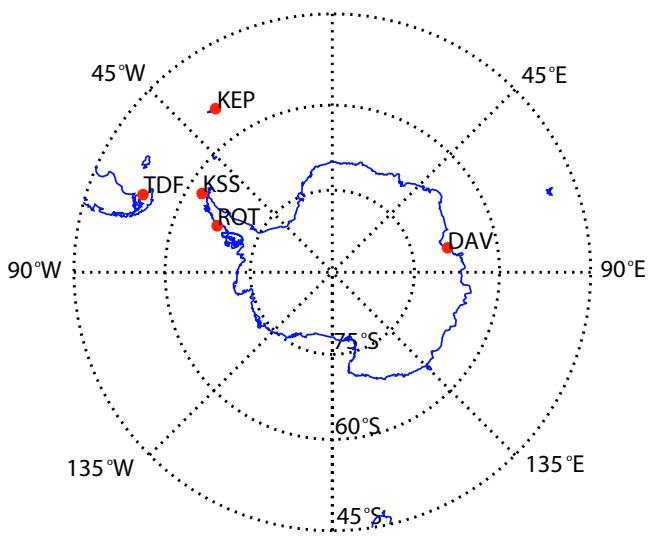

Figure 1. Projection of the meteor radar locations (shown as red dots).

3. Evaluation of NAVGEM-HA Results

3.1. Zonal and Meridional Winds

We first evaluate the NAVGEM-HA 3-hourly wind results for August and September of 2019. Vertical profiles of the analysis results have been converted to geometric altitude levels as described by Eckermann et al. (2009), and the profiles are selected for the latitude and longitude grids that are the closest to the meteor radar locations. For direct comparisons, the hourly winds from the corresponding radars are sampled every 3 hr and the subset obtained at the same times as the NAVGEM-HA results are used.

Figure 2 compares the time series of zonal winds at an altitude of ∼90 km for the two months over each of the radar locations. The analyzed winds resemble the radar observations, and the correlation coefficients between them are equal to 0.5 and 0.6 for most cases. The coefficients slightly decrease to be 0.4 and 0.3 over ROT and DAV for August, but for September the values are of ∼0.5 nearly identical to other stations. Overall, there is good agreement between the NAVGEM-HA and radar winds at this vertical level.

Similarly, Figure 3 presents the time series comparison for the meridional winds at the same altitude over these radar locations. The correlation coefficients are almost the same as those for the zonal winds, though show somewhat larger values in August over ROT and DAV. The values are also equal to 0.5 and 0.6 for September at all stations. Figure 3 shows again that the analyzed and observed winds are correlated with each other.

Figures 2 and 3 show that the 3-hourly time series generally agree between the NAVGEM-HA and radar winds, having a correlation for both zonal and meridional winds at the altitude in the MLT region. The correlation is noted in August and September including both non-SSW and SSW times, and for the SSW event in September a strong correlation is recognized. These demonstrate that the NAVGEM-HA system is able to capture most features of the observed winds and there is good agreement between the analysis results and the radar observations during the 2019 SSW condition.

The differences of the NAVGEM-HA winds from the measured values at ∼90 km are displayed in Figure 4. As shown, the differences are small at most times, and except for KEP in August the mean differences are all less than 10 m/s in both wind components. The mean differences are even smaller in the meridional wind component for September at only few m/s. The analysis results are thus close to the measurements, suggesting the ability of NAVGEM-HA to accurately represent the MLT winds. The small differences indicate that there are no large systematic biases in the NAVGEM-HA winds. However, the Root Mean Square (RMS) errors are much larger with the values between ∼25 and 35 m/s, being larger than the radar wind uncertainties. This indicates large variations in the NAVGEM-HA results, and some of these differences could be because the radars observe a broad area and the radar winds are more smoothed. The absolute differences appear to oscillate, changing between maximum and minimum values within a day. Indeed, Figure 5 shows that a ∼0.5-day periodic signature dominates at all stations. Longer periodic signatures are below the 95% statistically significant levels. The wind differences could thus be related to tides that are observed to attain large amplitudes in the Antarctic MLT region (e.g., Murphy et al., 2006).

To further examine the NAVGEM-HA and meteor radar agreement at different altitudes, Figure 6 plots the correlation coefficient, the mean difference and the RMS error between the NAVGEM-HA and radar winds from ∼80 to 98 km for both August and September of 2019. As noticed, below ∼90 km the correlation coefficients are mostly greater than 0.5 and the mean differences are approaching zero for both winds. The correlation decreases and the difference increases noticeably above 90 km altitude, and the RMS error increases, so the NAVGEM-HA analysis results agree better with the observations at ∼80–90 km. This is not surprising as most observational data assimilated in the system do not extend to above 90 km. For September, the absolute wind differences are rather similar across the vertical range for all stations and the difference values are almost the same as those in August below ∼90 km. This is consistent with findings that data assimilation improves the representation of the state of the MLT region during SSWs (e.g., Pedatella et al., 2018; Sassi et al., 2021).

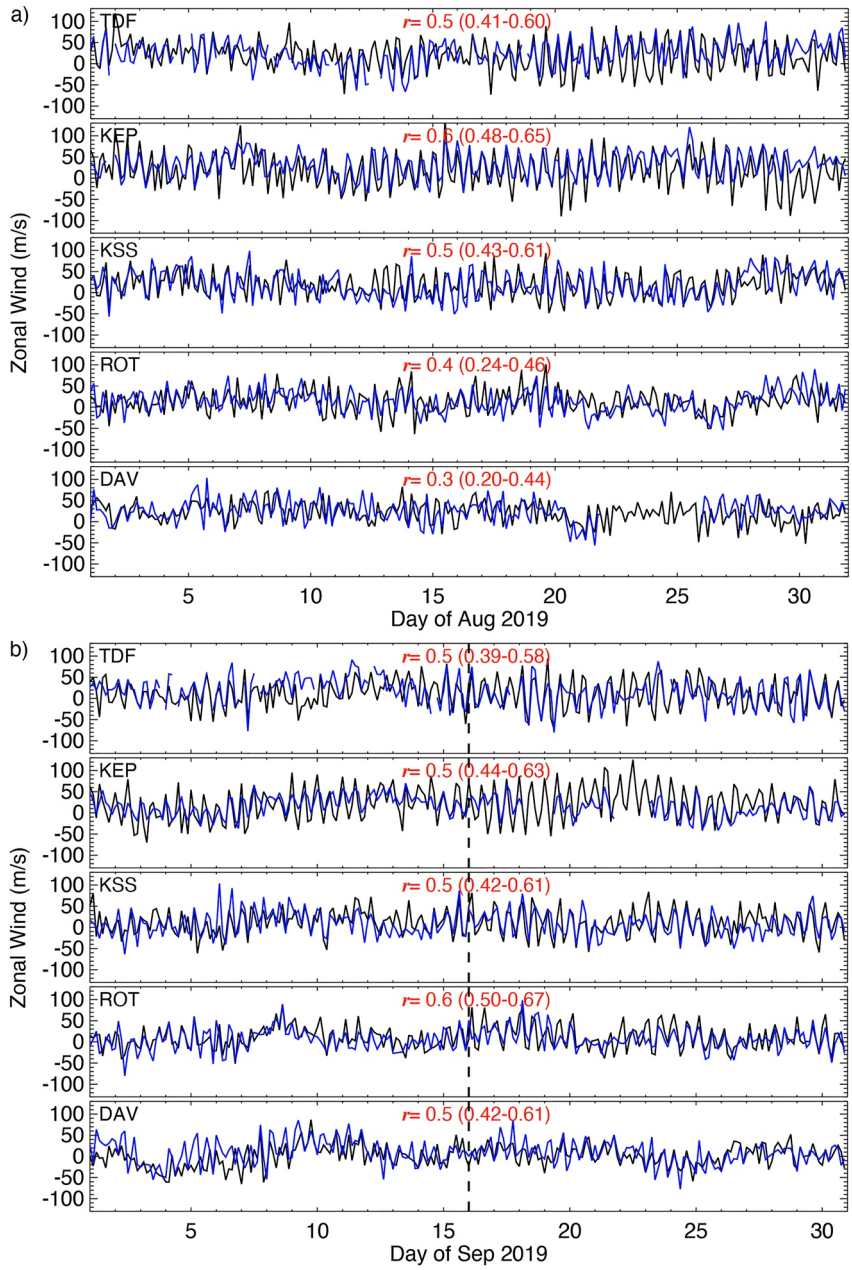

Figure 2. Three-hourly zonal winds at ~90 km altitude from the NAVGEM-HA results (black) and the radar measurements (blue) at the locations as denoted during (a) August and (b) September of 2019. The correlation coefficient *r* is given in red, and the lower and upper 95% confidence interval limits are in bracket. Vertical dashed line marks the SSW peak warming date on 16 September (SSW onset on 1 September) of 2019.

3.2. Wind and Tidal Variations During the SSW

We now turn our attention to the SSW effects and evaluate the wind evolution on a day-to-day basis during the 2019 Antarctic SSW. Daily averaged profiles of the zonal and meridional winds from the NAVGEM-HA results and the radars are compared in Figure 7 for the altitude range from ~80 to 98 km over 21 August–30 September of 2019. Both wind components display a similar pattern between these stations, and for each station the analyzed and observed wind profiles exhibit some similar features during this SSW.

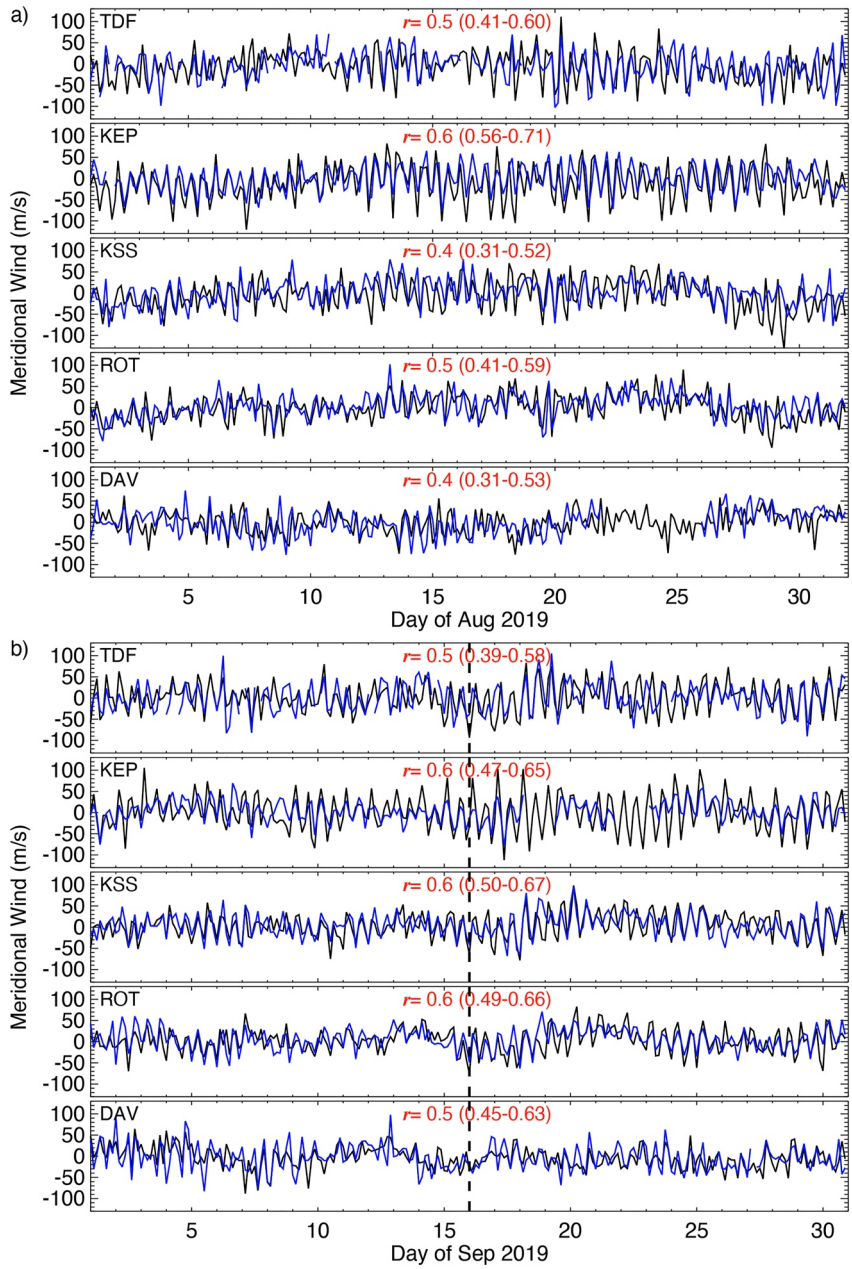

Figure 3. Same as Figure 2, but for the meridional winds.

Figure 7 indicates that the zonal winds are dominated by the eastward flows before the SSW and the winds reduce or even reverse the directions just few days after the SSW onset. Through the SSW, the zonal winds oscillate between the eastward and westward directions for every a few days, exhibiting a large wave signature. This signature could be related to planetary wave activities (e.g., Wang et al., 2021; Yu et al., 2019). The wind oscillations appear to continue into the peak warming, and following the SSW peak the eastward winds largely decrease to be a weak eastward flow or even turn the directions into the westward.

The meridional winds are also characterized by the alternating northward (equatorward) and southward (poleward) flows throughout the course of the SSW. Before the SSW, the winds are mostly poleward over TDF, KEP, KSS and ROT but equatorward over DAV. These poleward winds decrease and rapidly change to be in the equatorward direction immediately after the SSW onset. The rapid changes from the poleward to the equatorward

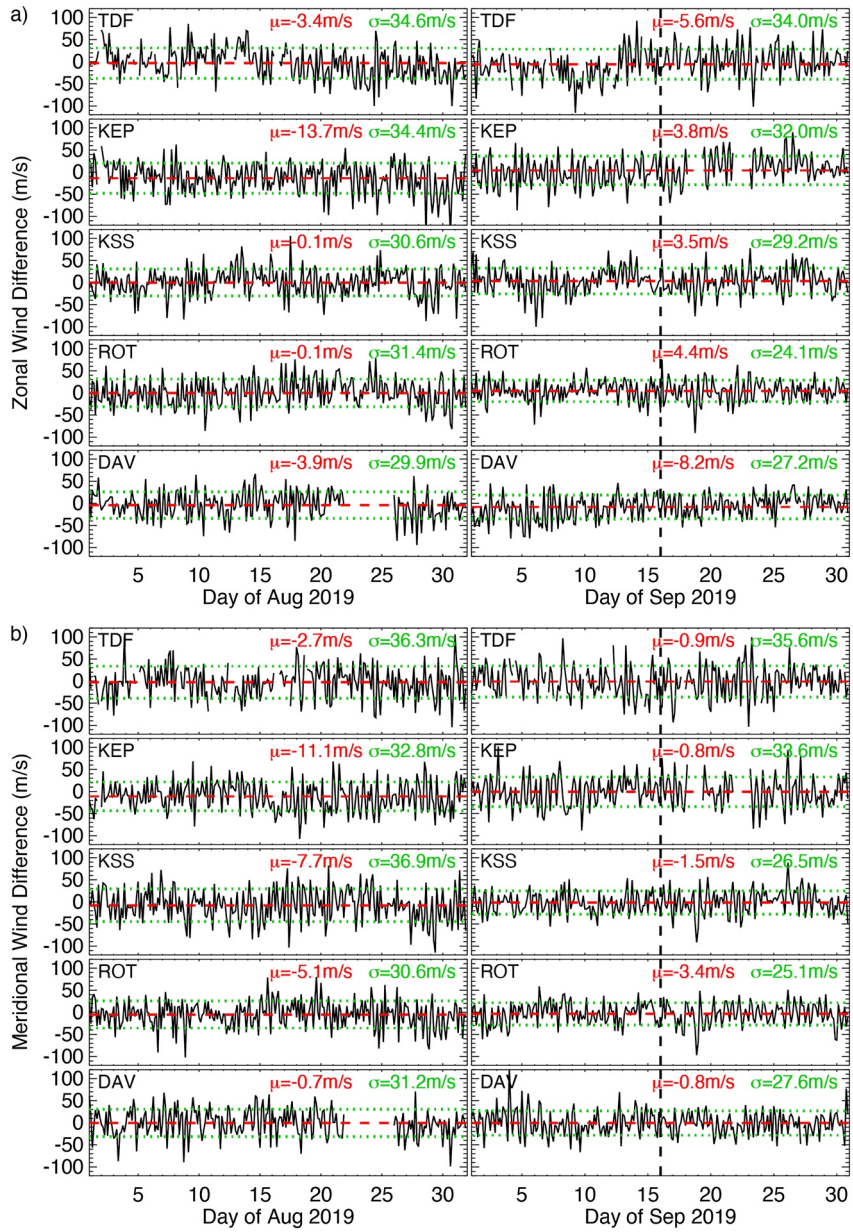

Figure 4. Differences of (a) zonal and (b) meridional winds at ~90 km altitude between the NAVGEM-HA results and the radar observations at the given locations during August (left panels) and September (right) of 2019. Red dashed line marks mean difference μ with the value provided, and green dotted line represents RMS error σ. Vertical dashed line marks the SSW peak on 19 September (SSW onset on 1 September).

winds are also noticed around the SSW peak. At DAV, the meridional winds are in the opposite direction to other stations. This is reasonable as that DAV is located almost on the opposite of the Drake Passage, being consistent with a global wave signature.

Figure 7 shows a similar variation pattern between the NAVGEM-HA wind profiles and the radar observations. This demonstrates again that the analysis system is able to capture large-scale day-to-day variations of the MLT winds during the 2019 SSW. However, there are some details that do not completely agree. For example, the eastward winds are observed to reach ~50 m/s over TDF on ~day 255 in the middle of the SSW, but the analyzed winds have the maximum values of only ~30 m/s at the same times. The differences are also recognized at other

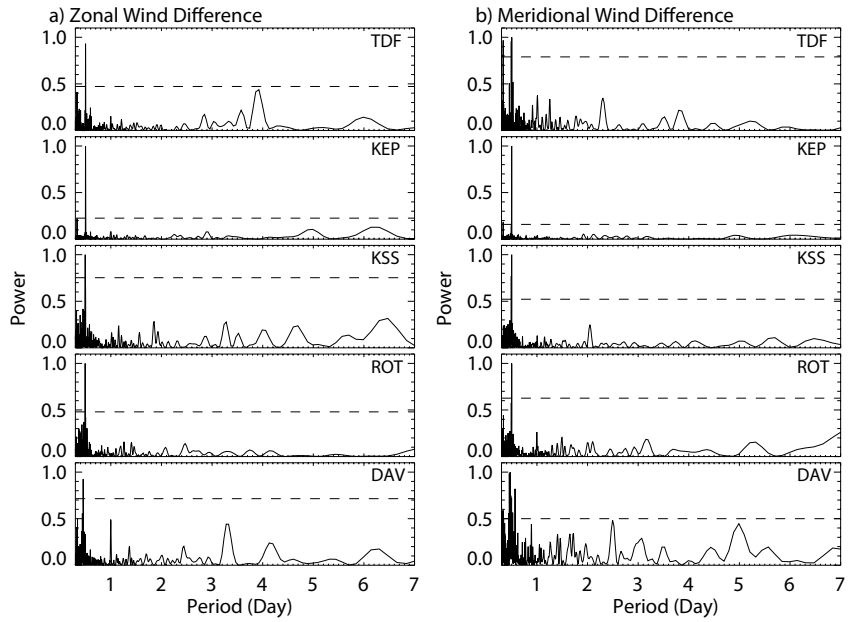

Figure 5. Normalized periodogram of the wind differences between NAVGEM-HA and the radars for (a) zonal and (b) meridional winds at ~90 km altitude during 1 August to 30 September 2019. Horizontal dashed line marks the 95% significance level.

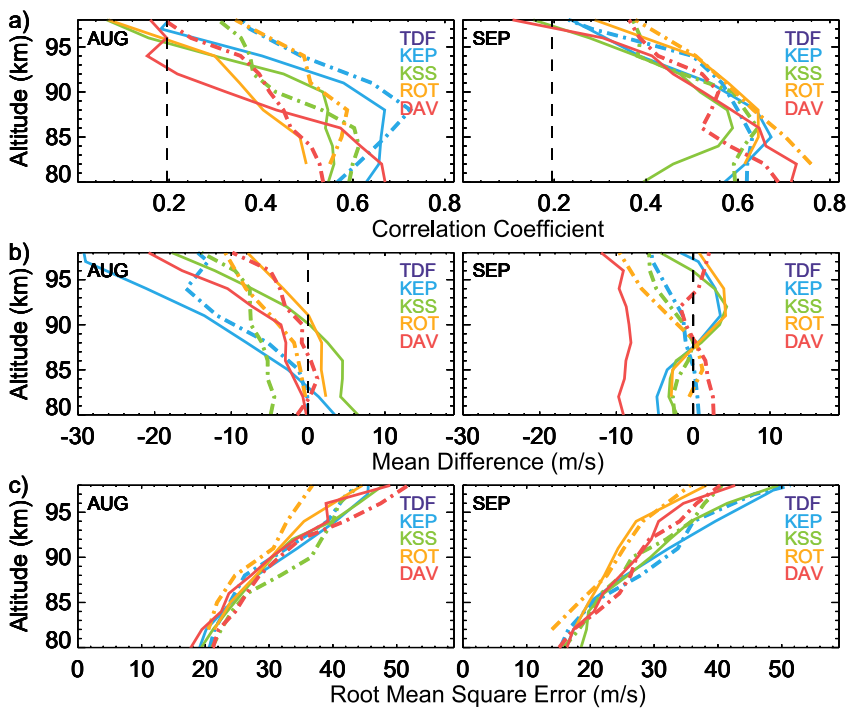

Figure 6. (a) Correlation coefficient, (b) mean difference, and (c) RMS error between the NAVGEM-HA and radar winds for the zonal (solid line) and meridional (dot dashed line) wind components over various locations (in different colors), presented vs. altitude from ~80 to 98 km. Black vertical dashed lines mark the 95% critical value of the sample correlation coefficient at 0.195 and the zero difference.

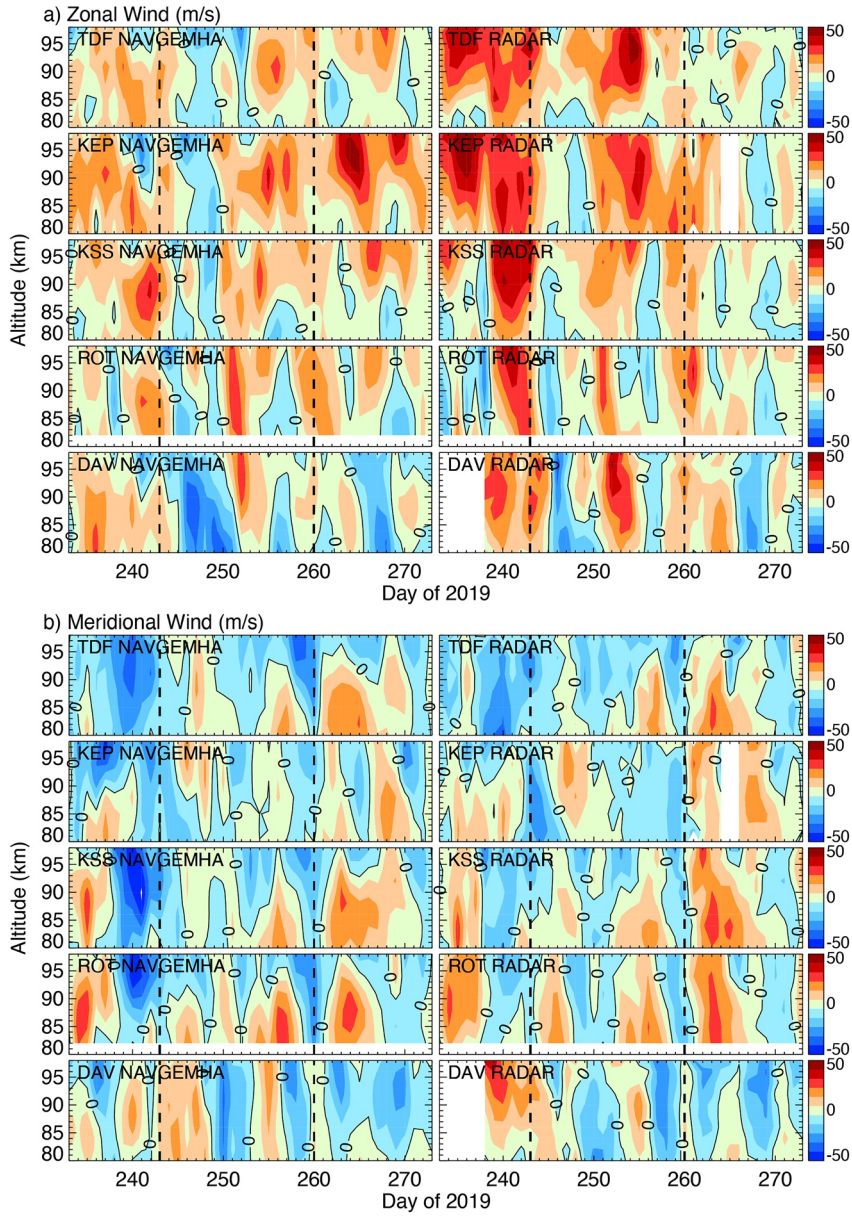

Figure 7. Daily mean (a) zonal and (b) meridional winds from NAVGEM-HA (left panels) and the radars (right) over the radar locations, presented versus altitude from ~80 to 98 km during 21 August–30 September 2019 (day 233–273). Vertical dashed lines mark the SSW onset and peak warming dates on 1 and 16 September (day 243 and 260). White area represents missing data.

stations and in the meridional winds. In addition, there are small altitude variations and structures that are not fully captured by the NAVGEM-HA analysis system.

Figure 8 further compares the daily mean winds averaged between ~80 and 90 km altitude during the 2019 SSW event from 21 August to 30 September 2019. The NAVGEM-HA winds are more reliable in this altitude range (refer to Figure 6), and the averaged results reveal mostly the day-to-day variations in response to the SSW. The wind behavior is clear, including the decrease of the eastward wind at both the SSW onset and the SSW peak. Correspondingly, the meridional winds reverse their directions, changing from the poleward winds to be the equatorward flows few days after the SSW onset and on the peak warming day. At DAV, the meridional winds are in the opposite directions and the winds change from the equatorward to the poleward directions during this SSW.

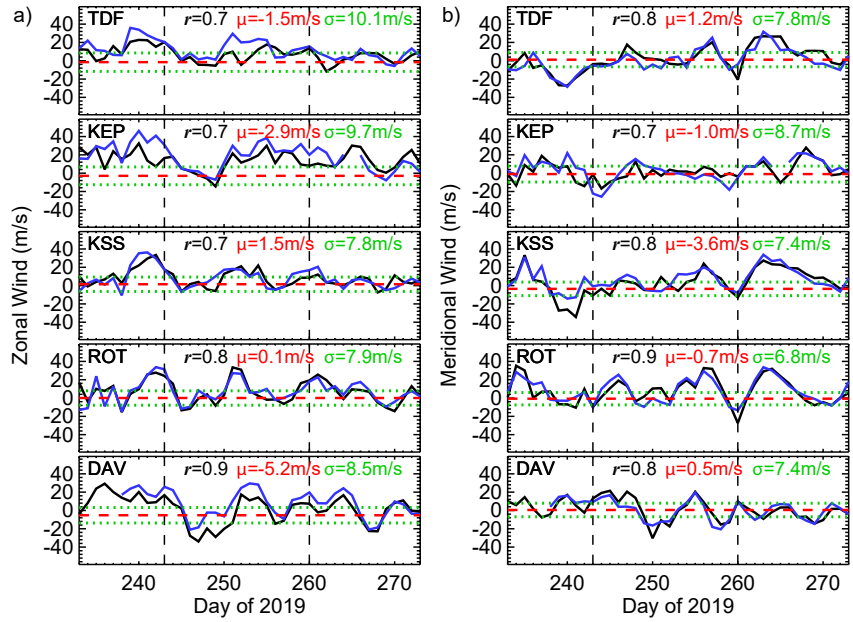

Figure 8. Daily mean (a) zonal and (b) meridional winds averaged between ~80 and 90 km altitude from NAVGEM-HA (black) and the radars (blue) during 21 August–30 September 2019. Horizontal red dashed line marks mean wind difference μ, and green dotted line represent RMS error σ. Correlation coefficient r is also provided. Vertical dashed lines mark the SSW onset and peak warming dates on 1 and 16 September (day 243 and 260).

Figure 8 also shows that the series of daily mean winds are highly correlated between the NAVGEM-HA results and the radars, having the coefficients of 0.7–0.9 among these different stations and for both wind components. The daily mean differences are all small with the largest values of only ~5 m/s over DAV for the zonal wind component. The wind differences are even smaller at other stations, and for both wind components the mean differences are equal to only few m/s. Similarly, the RMS errors also decrease being much smaller than the 3-hourly wind results (see Figures 2–4). These daily averaged winds have better agreement with the observations, indicating that shorter timescale variations such as those related to semidiurnal and diurnal variations may not be precisely captured in the NAVGEM-HA wind fields.

Figures 9a and 9b illustrate the composite zonal and meridional winds from the 3-hourly NAVGEM-HA results and the hourly radar measurements averaged over the time interval from 21 August to 30 September 2019. The maximum and minimum winds slightly differ between NAVGEM-HA and the radars for the corresponding locations, and the altitudes and times of these maxima and minima do not exactly agree. These suggest again that NAVGEM-HA does not completely describe short timescale variations. The winds over DAV show somewhat different patterns between NAVGEM-HA and the observations, which is possible given that less observational data are assimilated as the SABER observations do not cover this latitude during the time interval. However, both the analyzed and observed winds show a clear pattern with two wind maxima and minima separated by ~12 hr in both zonal and meridional wind components.

For each location, the wind maximum and minimum shift to appear at earlier times at higher altitudes. This indicates that the phase of this 12-hr oscillation decreases with increasing altitude, and this phase change is consistent with the upward propagation. The phase shifts by ~2–3 hr within this ~18 km altitude range, so the vertical wavelength of the oscillation is equal to ~70–100 km. The phase also shifts between different stations, changing with the longitude of the radar location. Specifically, the wind peaks later at TDF than KEP by ~2 hr. Given that TDF and KEP are located at similar latitudes and TDF is on the west of KEP with the longitude difference of ~30° (TDF is at ~68°W and KEP is at ~37°W), the 12-hr oscillation propagates westward at the phase speed of ~15° longitude/hour (360°/day). The wind maxima are the strongest at TDF and KEP, and are weaker at ROT and DAV at higher latitudes, showing the amplitude change of the oscillation with latitude. These features are all consistent with properties of semidiurnal tides reported before (e.g., Murphy et al., 2006; Stober et al., 2021).

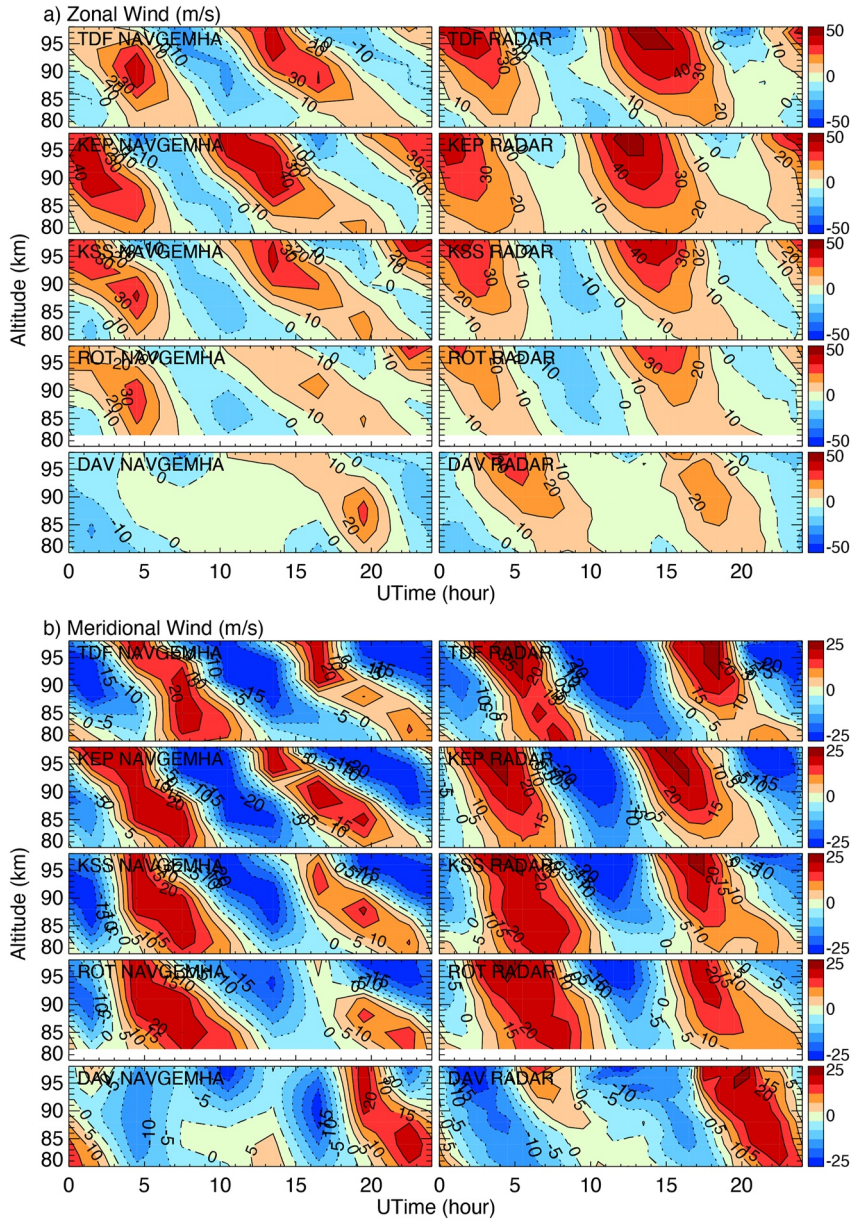

Figure 9. Composite (a) zonal and (b) meridional winds at the radar locations from 3-hourly NAVGEM-HA output (left panels) and hourly radar measurements (right) throughout 21 August–30 September 2019.

Figure 10 compares the mean amplitudes and phases of semidiurnal tides between NAVGEM-HA and the radars as a function of altitude from ~80 to 98 km. At each altitude, a least-squares fit to 24-, 12-, 8-, and 6-hr cycles has been applied to the analyzed (3-hourly) and observed (hourly) winds for each day, and the daily amplitudes and phases obtained for the 12-hr tides are averaged over the time interval from 21 August to 30 September 2019.

Figure 10 shows that the semidiurnal tidal amplitudes from NAVGEM-HA are greater than those observed by the radars at TDF, KEP, and KSS but the tidal amplitudes are similar at ROT and DAV. The analyzed tides have the largest amplitudes peaking at ~90 km altitude whereas the observations show that the amplitude increases with altitude. These are noticed in both zonal and meridional winds, and the tidal amplitude differences appear to be larger at higher altitudes above ~90 km. These differences are expected as the NAVGEM-HA winds are more reliable between ~80 and 90 km (see Figure 6). The tidal phases are fairly consistent between the NAVGEM-HA

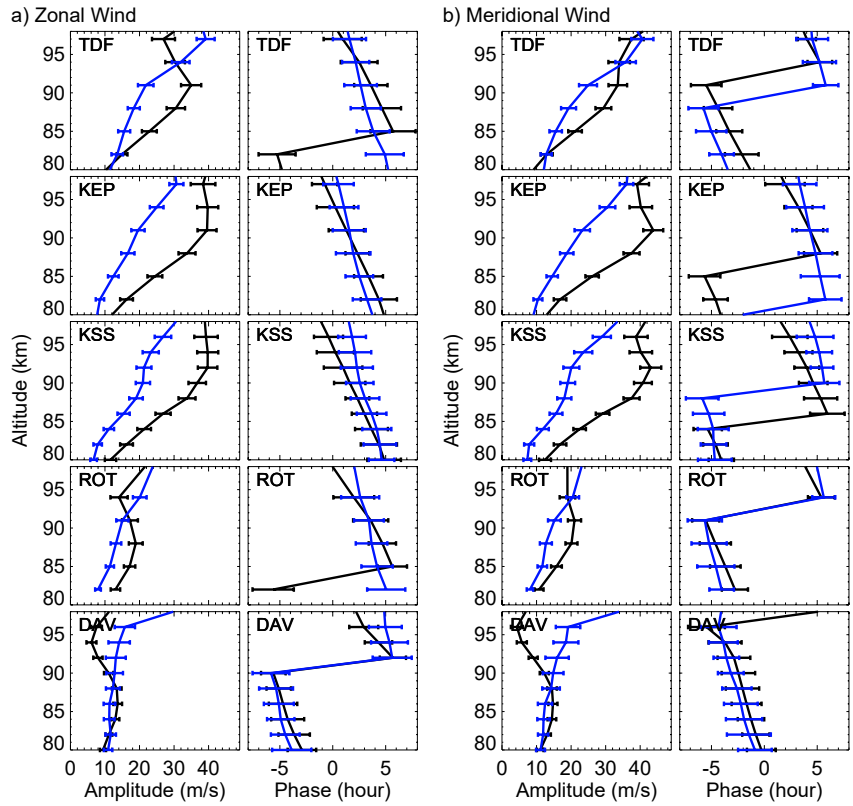

Figure 10. Amplitudes and phases of semidiurnal tides from NAVGEM-HA (black) and the radars (blue) in (a) zonal and (b) meridional winds over the given locations, averaged from 21 August to 30 September 2019. Horizontal bars represent the standard errors.

results and the radars, and both show decreasing phase with increasing altitude suggesting again the upward propagation of semidiurnal tides in the MLT region.

Similarly, Figure 11 presents the mean amplitudes and phases of diurnal tides during the SSW. Daily tidal amplitudes and phases are averaged over the time interval and presented as a function of altitude from ∼80 to 98 km. These diurnal tides have much smaller amplitudes than semidiurnal tides, being several times smaller and reaching the largest amplitudes of only ∼10 m/s in both zonal and meridional winds. The analyzed diurnal tidal amplitudes mostly agree with the observed values though there remain some differences specifically for high altitudes above 90 km. Also, the diurnal tidal phases are consistent between the NAVGEM-HA results and the radar observations, and the phase decreases with increasing altitude suggesting the upward propagation.

Next, we investigate the tidal behavior during this 2019 SSW. Figure 12 provides the daily amplitudes of diurnal and semidiurnal tides at ∼90 km altitude from the NAVGEM-HA winds and the radar measurements throughout the time interval from 21 August to 30 September 2019. The NAVGEM-HA results do not completely match the observations, but both the analyzed and observed tidal amplitudes show a large increase around the peak of the SSW on day 260 (16 September). Such a tidal enhancement is seen for both diurnal and semidiurnal tides and in zonal and meridional winds. This variation is most evident at TDF and KEP, and the signature is relatively weaker at ROT and DAV suggesting the latitudinal difference.

Previous studies have reported the amplification of tides during SSWs in the NH (e.g., Jin et al., 2012; Lieberman et al., 2015; Pedatella et al., 2014). The tidal enhancement identified here from the NAVGEM-HA system and the radars is thus as expected. NAVGEM-HA has been used to investigate the tidal variability on both short-term and interannual scales and comparisons with TIMED/SABER have shown a similar variation pattern in temperature

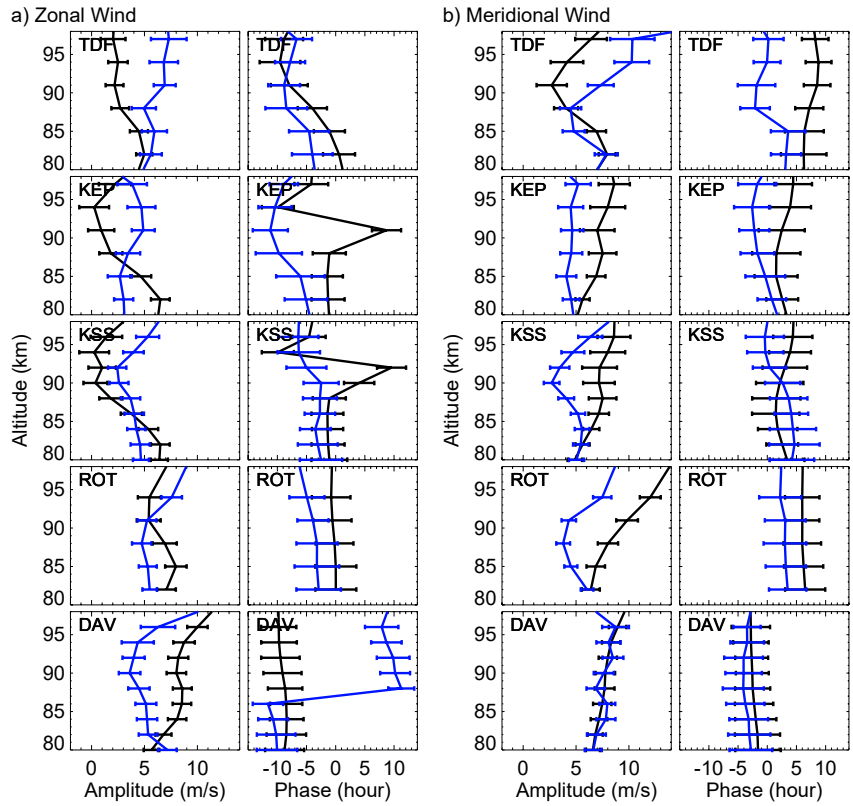

Figure 11. Same as Figure 10, but for diurnal tides.

(Dhadly et al., 2018). This study identifies the tidal response to the Antarctic SSW in the wind fields near 60° latitude in the SH.

The tidal variations during SSWs could be due to a number of possible mechanisms: (a) Changes in the zonal mean zonal winds that affect the vertical propagation of tides in the MLT region (e.g., Ekanayake et al., 1997; Jin et al., 2012; Pedatella et al., 2012); (b) Ozone changes (e.g., Goncharenko et al., 2012; Siddiqui et al., 2019); (c) Nonlinear interaction of stationary planetary waves with tides (e.g., Lieberman et al., 2015). Other mechanisms such as interaction between tides and traveling planetary waves (e.g., McCormack et al., 2010), spatially varying winds (e.g., McLandress, 2002) and lunar tides (e.g., Pedatella et al., 2012) could also be responsible.

We have used the NAVGEM-HA output to examine some of these processes. Figure 13a shows during this 2019 SH SSW the zonal mean ozone mixing ratio at 2.5 hPa (~40 km altitude), at the level close to the peak heating of tidal generations. The ozone mixing ratio is the largest at ~50°S latitude, and the value increases rapidly around the SSW peak on day 260, being overlapped with the enhancements of tidal amplitudes seen in this study.

Large changes in migrating tides during SSWs have been reported before (e.g., Fuller-Rowell et al., 2010). Theoretically, these tides interact with stationary planetary waves (PWs), producing nonmigrating tides (e.g., Angelats I Coll & Forbes, 2002; Lieberman et al., 2015; Teitelbaum & Vial, 1991). Amplification of nonmigrating tides due to the PW-tide interaction has been verified using observations and simulations for the NH (e.g., Chang et al., 2009; Liu et al., 2010; Pancheva et al., 2009; Pedatella & Liu, 2013; Pedatella et al., 2012; Stober, Baumgarten, et al., 2020). Figure 13b presents the PW-1 amplitudes and the semidiurnal migrating (SW2) and nonmigrating (SW3 and SW1) tides extracted from the full NAVGEM-HA output over this 2019 SH SSW. As shown, the stratospheric PW-1 amplitude decreases largely before the SSW peak (~day 260) and then recovers immediately after the peak warming date. SW2 and SW3 at ~90 km altitude have similar changes

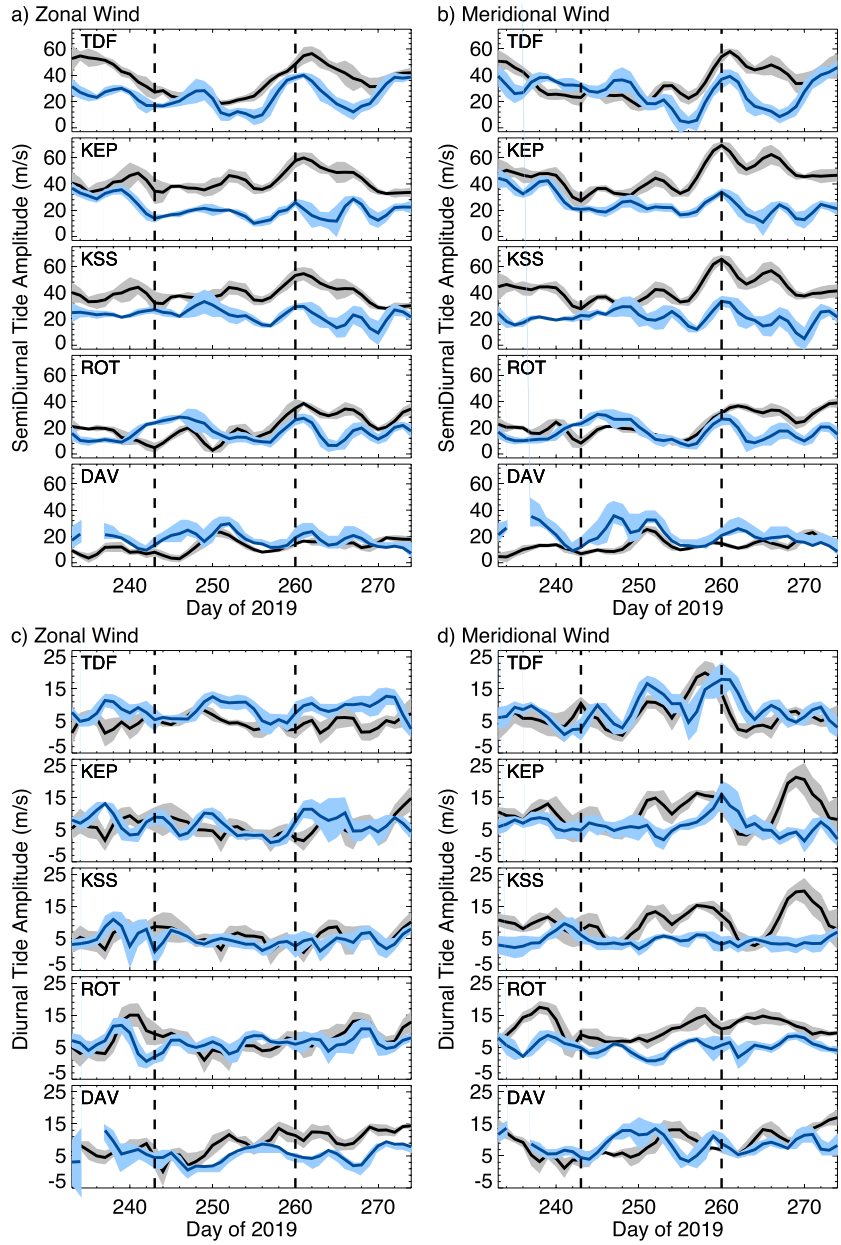

Figure 12. Amplitudes of semidiurnal (a) and (b) and diurnal tides (c) and (d) in the zonal (left panels) and meridional (right) winds at ~90 km altitude from NAVGEM-HA (black) and the radars (blue) at the given locations throughout 21 August–30 September 2019. Daily tidal amplitudes have been averaged through a 3-day running window stepped by one day. Shadow is for one sigma of the 3-day running mean. Vertical dashed lines mark the SSW onset and peak warming dates on 1 and 16 September (day 243 and 260).

and both exhibit the amplitude enhancement in respond to the minor enhancement in PW-1 after the SSW peak. SW1 shows similarities to SW2 and SW3 through the course of the SSW, but the SW1 amplitude decreases largely following the peak SSW. Nonetheless, the similar variability between SW2 and SW3 and their amplitude enhancements during the SSW peak are consistent with that SW3 nonmigrating tides are produced by the PW-tide interaction. This study reveals evidence on the PW-tide interaction, and suggests that the same process holds in the SH. However, this study focuses on the evaluation of the NAVGEM-HA wind fields, and its tidal response to the 2019 Antarctic SSW. Examining the detailed processes for causing the tidal variations is beyond the scope of this study.

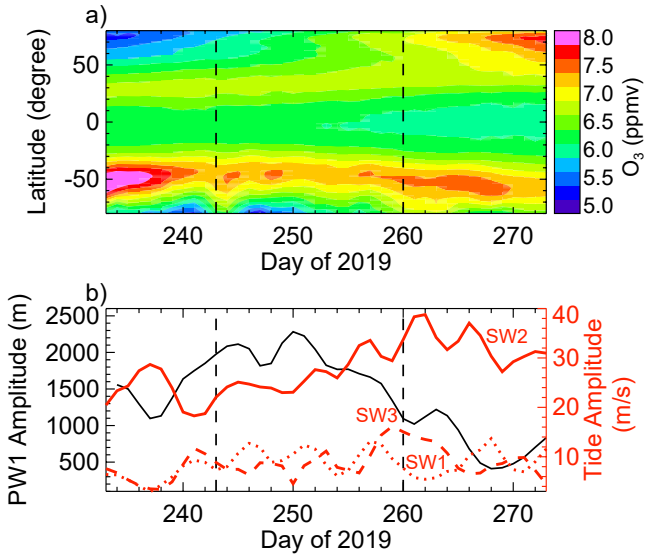

Figure 13. (a) Daily averaged zonal mean ozone mixing ratio at ~40 km altitude, and (b) PW-1 geopotential height amplitude at ~30 km at 60°S latitude (black line), and SW2 (solid red), SW3 (dashed red) and SW1 (dotted red) tidal amplitudes in zonal wind at ~90 km over 60°S latitude from the NAVGEM-HA global output during 21 August–30 September 2019. Vertical dashed lines mark the SSW onset and peak warming dates on 1 and 16 September (day 243 and 260).

4. Summary and Conclusions

This study assesses MLT winds produced by the NAVGEM-HA meteorological analysis with data assimilation for August and September 2019 including the entire Antarctic SSW event. The analyzed winds are compared to the meteor radar measurements at five stations across SH mid-to-high latitudes. One-to-one comparisons are made for both zonal and meridional winds, and both 3-hourly and daily averaged results are evaluated. The study also reports the tidal behavior on daily basis during the SH SSW.

In general, the comparison demonstrates that the NAVGEM-HA analysis of MLT winds near 60°S latitude agree well with the radar observations in the vertical range from ~80 to 90 km when averaged over 24 hr. NAVGEM-HA is able to capture the large day-to-day variations related to tidal motions. Both the analyzed and observed winds show enhancements in diurnal and semidiurnal tidal amplitudes following the peak of the 2019 SH SSW. The analysis results suggest that enhancements in nonmigrating tides around the SSW peak could be produced through the interaction of migrating tides with stationary planetary waves. However, the NAVGEM-HA winds do not completely match the radar observations and shorter-term variations are not well represented. Moreover, the analysis system overestimates semidiurnal tidal amplitudes at some locations, and the daily evolutions of tides are not identical to the results from the radars. These suggest that challenges remain to fully describe the state of the MLT region and reproduce the variability observed at SH mid-to-high latitudes. More work is still needed to improve the numerical representation of the MLT winds and tides in response to the SSW.

Data Availability Statement

The NAVGEM-HA results evaluated in this study are publicly available at https://map.nrl.navy.mil/map/pub/nrl/navgem2019/. The meteor radar data are accessible at the CEDAR Madrigal Database at http://millstonehill.haystack.mit.edu. Data from King Edward Point and Rothera are archived at the Centre for Environmental Data Archival (CEDA) and are freely available at https://data.ceda.ac.uk/badc/meteor-radars/data. The metadata for the Davis station are accessible at https://data.aad.gov.au/metadata/Davis_33MHz_Meteor_Radar.

Acknowledgments

Dr. John McCormack provided the NAVGEM-HA analysis and contributed to the evaluation of the data and the drafting of the manuscript. We thank him for valuable discussions and suggestions. The operation of the SAAMER radar at Tierra del Feugo is supported by NASA SSO program and NESC assessment T1-17-0120. The authors appreciate the invaluable support of Jose Luis Hormaechea, Carlos Ferrer, Gerardo Connon, Luis Barbero, and Leandro Mazlov with the operation of SAAMER. SAAMER operations are partially supported through a Memorandum of Understanding between the University of La Plata and the Catholic University of America. We would like to thank the government of South Georgia and the South Sandwich Islands for their cooperation. The King Edward Point (KEP) and Rothera radars were supported by the Natural Environment Research Council (NERC) under Grants NE/K015117/1, NE/R001235/1, NE/R001391/1, and

References

Alexander, M. J., Gille, J., Cavanaugh, C., Coffey, M., Craig, C., Eden, T., et al. (2008). Global estimates of gravity wave momentum flux from high resolution dynamics limb sounder observations. *Journal of Geophysical Research*, *113*, D15S18. https://doi.org/10.1029/2007JD008807

Angelats I Coll, M., & Forbes, J. M. (2002). Nonlinear interactions in the upper atmosphere: The s = 1 and s = 3 nonmigrating semidiurnal tides. *Journal of Geophysical Research*, *107*(A8), 1157. https://doi.org/10.1029/2001ja900179

Becker, E., & Vadas, S. L. (2018). Secondary gravity waves in the winter mesosphere: Results from a high-resolution global circulation model. *Journal of Geophysical Research*, *123*, 2605–2627. https://doi.org/10.1002/2017jd027460

Chang, L. C., Palo, S. E., & Liu, H.-L. (2009). Short-term variation of the s =1 nonmigrating semidiurnal tide during the 2002 stratospheric sudden warming. *Journal of Geophysical Research*, *114*, D03109. https://doi.org/10.1029/2008JD010886

Chau, J. L., Goncharenko, L. P., Fejer, B. G., & Liu, H.-L. (2012). Equatorial and low latitude ionospheric effects during sudden stratospheric warming events. *Space Science Reviews*, *168*(1–4), 385–417. https://doi.org/10.1007/s11214-011-9797-5

de Wit, R., Janches, D., Fritts, D. C., Stockwell, R. G., & Coy, L. (2017). Unexpected climatological behavior of MLT gravity wave momentum flux in the Lee of the Southern Andes hotspot. *Geophysical Research Letters*, *44*, 1182–1191. https://doi.org/10.1002/2016gl072311

Dhadly, M. S., Emmert, J. T., Drob, D. P., McCormack, J. P., & Niciejewski, R. (2018). Short-term and interannual variations of migrating diurnal and semidiurnal tides in the mesosphere and lower thermosphere. *Journal of Geophysical Research*, *123*, 7106–7123. https://doi.org/10.1029/2018JA025748

Dowdy, A., Vincent, R. A., Murphy, D. J., Tsutsumi, M., Riggin, D. M., & Jarvis, M. J. (2004). The large scale dynamics of the mesosphere-lower thermosphere during the Southern Hemisphere stratospheric warming of 2002. *Geophysical Research Letters*, *31*, L14102. https://doi.org/10.1029/2004gl020282

Eckermann, S. D., Hoppel, K. W., Coy, L., McCormack, J. P., Siskind, D. E., Nielsen, K., et al. (2009). High-altitude data assimilation system experiments for the northern summer mesosphere season of 2007. *Journal of Atmospheric and Solar-Terrestrial Physics*, *71*, 531–551. https://doi.org/10.1016/j.jastp.2008.09.036

Eckermann, S. D., Ma, J., Hoppel, K. W., Kuhl, D. D., Allen, D. R., Doyle, J. A., et al. (2018). High-altitude (0–100 km) global atmospheric reanalysis system: Description and application to the 2014 austral winter of the deep propagating gravity wave experiment (DEEPWAVE). *Monthly Weather Review*, *146*, 2639–2666. https://doi.org/10.1175/mwr-d-17-0386.1

NE/K012614. The South Georgia meteor radar at KEP was installed by N. J. Mitchell and BAS in 2016, and it was supported by the SGWEX and DRAGON-WEX grants for which N. J. Mitchell and T. Moffat-Griffin were investigators. J.-H. Kim and C. Lee were supported by the Grant PE22020 from Korea Polar Research Institute. Support for the operation of the Davis meteor radar has been provided through Australian Antarctic Science project 4445. J. Ma was partially supported by NASA's Heliophysics Guest Investigator Program NNH19ZDA001N-HGIO.

Eckermann, S. D., Wu, D. L., Doyle, J. D., Burris, J. F., McGee, T. J., Hostetler, C. A., et al. (2006). Imaging gravity waves in lower stratospheric AMSU-A radiances, Part 2: Validation case study. *Atmospheric Chemistry and Physics*, *6*, 3343–3362. https://doi.org/10.5194/acp-6-3343-2006

Ekanayake, E. M. P., Aso, T., & Miyahara, S. (1997). Background wind effect on propagation of nonmigrating diurnal tides in the middle atmosphere. *Journal of Atmospheric and Solar-Terrestrial Physics*, *59*, 401–429. https://doi.org/10.1016/s1364-6826(96)00012-0

England, S. L., Maus, S., Immel, T. J., & Mende, S. B. (2006). Longitudinal variation of the E-region electric fields caused by atmospheric tides. *Geophysical Research Letters*, *33*, L21105. https://doi.org/10.1029/2006GL027465

Ern, M., Preusse, P., Alexander, M. J., & Warner, C. D. (2004). Absolute values of gravity wave momentum flux derived from satellite data. *Journal of Geophysical Research*, *109*, D20103. https://doi.org/10.1029/2004JD004752

Forbes, J. M., Zhang, X., Palo, S., Russell, J., Mertens, C. J., & Mlynczak, M. (2008). Tidal variability in the ionospheric dynamo region. *Journal of Geophysical Research*, *113*, A02310. https://doi.org/10.1029/2007JA012737

Fritts, D. C., Iimura, H., Janches, D., Lieberman, R. S., Riggin, D. M., Mitchell, N. J., et al. (2019). Structure, variability, and mean-flow interactions of the January 2015 Quasi-2-Day wave at middle and high southern latitudes. *Journal of Geophysical Research*, *124*, 5891–6008. https://doi.org/10.1029/2018jd029728

Fritts, D. C., Janches, D., & Hocking, W. K. (2010). Southern Argentina agile meteor radar: Initial assessment of gravity wave momentum fluxes. *Journal of Geophysical Research*, *115*, D19123. https://doi.org/10.1029/2010JD013891

Fritts, D. C., Janches, D., Iimura, H., Hocking, W. K., Mitchell, N. J., Stockwell, R. G., et al. (2010). Southern Argentina agile meteor radar: System design and initial measurements of large-scale winds and tides. *Journal of Geophysical Research*, *115*, D18112. https://doi.org/10.1029/2010JD013850

Fuller-Rowell, T., Wu, F., Akmaev, R., Fang, T.-W., & Araujo-Pradere, E. (2010). A whole atmosphere model simulation of the impact of a sudden stratospheric warming on thermosphere dynamics and electrodynamics. *Journal of Geophysical Research*, *115*, A00G08. https://doi.org/10.1029/2010JA015524

Garcia, R. R., Smith, A. K., Kinnison, D. E., de La Cámara, Á., & Murphy, D. J. (2017). Modification of the gravity wave parameterization in the whole atmosphere community climate model: Motivation and results. *Journal of the Atmospheric Sciences*, *74*, 275–291. https://doi.org/10.1175/jas-d-16-0104.1

Goncharenko, L. P., Coster, A. J., Plumb, R. A., & Domeisen, D. I. (2012). The potential role of stratospheric ozone in the stratosphere-ionosphere coupling during stratospheric warmings. *Geophysical Research Letters*, *39*, L08101. https://doi.org/10.1029/2012GL051261

Goncharenko, L. P., Havey, V. L., Greer, K. R., Zhang, S.-R., Coster, A. J., & Paxton, L. J. (2021). Impact of September 2019 Antarctic sudden stratospheric warming on mid-latitude ionosphere and thermosphere over North America and Europe. *Geophysical Research Letters*, *48*, e2021GL094517. https://doi.org/10.1029/2021GL094517

Guest, F. M., Reeder, M. J., Marks, C. J., & Karoly, D. J. (2000). Inertia gravity waves observed in the lower stratosphere over Macquarie Island. *Journal of Atmospheric Science*, *57*, 737–752. https://doi.org/10.1175/1520-0469(2000)057<0737:igwoit>2.0.co;2

Hagan, M. E., Burrage, M. D., Forbes, J. M., Hackney, J., Randel, W. J., & Zhang, X. (1999). GSWM-98: Results for migrating solar tides. *Journal of Geophysical Research*, *104*(A4), 6813–6827. https://doi.org/10.1029/1998ja900125

Hagan, M. E., & Forbes, J. M. (2003). Migrating and nonmigrating semidiurnal tides in the upper atmosphere excited by tropospheric latent heat release. *Journal of Geophysical Research*, *108*(A2), 1062. https://doi.org/10.1029/2002JA009466

Hertzog, A., Boccara, G., Vincent, R. A., Vial, F., & Cocquerez, P. (2008). Estimation of gravity wave momentum flux and phase speeds from quasi-Lagrangian stratospheric balloon flights. Part II: Results from the Vorcore campaign in Antarctica. *Journal of Atmospheric Science*, *65*, 3056–3070. https://doi.org/10.1175/2008jas2710.1

Hibbins, R. E., Espy, P. J., Orsolini, Y. J., Limpasuvan, V., & Barnes, R. J. (2019). SuperDARN observations of semidiurnal tidal variability in the MLT and the response to sudden stratospheric warming events. *Journal of Geophysical Research*, *124*, 4862–4872. https://doi.org/10.1029/2018jd030157

Hogan, T., Liu, M., Ridout, J., Peng, M., Whitcomb, T., Ruston, B., et al. (2014). The navy global environmental model. *Oceanography*, *27*, 116–125. https://doi.org/10.5670/oceanog.2014.73

Holdsworth, D. A., Murphy, D. J., Reid, I. M., & Morris, R. J. (2008). Antarctic meteor observations using the Davis MST and meteor radars. *Advances in Space Research*, *42*, 143–154. https://doi.org/10.1016/j.asr.2007.02.037

Hoppel, K. W., Eckermann, S. D., Coy, L., Nedoluha, G. E., Allen, D. R., Swadley, S. D., & Baker, N. L. (2013). Evaluation of SSMIS upper atmosphere sounding channels for high-altitude data assimilation. *Monthly Weather Review*, *141*(10), 3314–3330. https://doi.org/10.1175/mwr-d-13-00003.1

Jiang, J. H., Wu, D. L., & Eckermann, S. D. (2002). Upper atmosphere research satellite (UARS) MLS observation of mountain waves over the Andes. *Journal of Geophysical Research*, *107*(D20), 8273. https://doi.org/10.1029/2002JD002091

Jin, H., Miyoshi, Y., Pancheva, D., Mukhtarov, P., Fujiwara, H., & Shinagawa, H. (2012). Response of migrating tides to the stratospheric sudden warming in 2009 and their effects on the ionosphere studied by a whole atmosphere-ionosphere model GAIA with COSMIC and TIMED/SABER observations. *Journal of Geophysical Research*, *117*, A10323. https://doi.org/10.1029/2012JA017650

Kim, J.-H., Kim, Y. H., Lee, C.-S., & Jee, G. (2010). Seasonal variation of meteor decay times observed at King Sejong Station (62.22°S, 58.78°W), Antarctica. *Journal of Atmospheric and Solar-Terrestrial Physics*, *72*(11–12), 883–889. https://doi.org/10.1016/j.jastp.2010.05.003

Lee, C., Kim, Y. H., Kim, J.-H., Jee, G., Won, Y.-I., & Wu, D. L. (2013). Seasonal variation of wave activities near the mesopause region observed at King Sejong Station (62.22°S, 58.78°W), Antarctica. *Journal of Atmospheric and Solar-Terrestrial Physics*, *105/106*, 30–38. https://doi.org/10.1016/j.jastp.2013.07.006

Lieberman, R. S., Oberheide, J., Hagan, M. E., Remsberg, E. E., & Gordley, L. L. (2004). Variability of diurnal tides and planetary waves during November 1978-May 1979. *Journal of Atmospheric and Solar-Terrestrial Physics*, *66*, 517–528. https://doi.org/10.1016/j.jastp.2004.01.006

Lieberman, R. S., Riggin, D. M., Ortland, D. A., Oberheide, J., & Siskind, D. E. (2015). Global observations and modeling of nonmigrating diurnal tides generated by tide-planetary wave interactions. *Journal of Geophysical Research*, *120*, 11419–11437. https://doi.org/10.1002/2015JD023739

Liu, G., Janches, D., Lieberman, R. S., Moffat-Griffin, T., Mitchell, N. J., Kim, J.-H., & Lee, C. (2021). Wind variations in the mesosphere and lower thermosphere near 60°S latitude during the 2019 Antarctic sudden stratospheric warming. *Journal of Geophysical Research*, *126*, e2020JA028909. https://doi.org/10.1029/2020ja028909

Liu, G., Lieberman, R. S., Harvey, V. L., Pedatella, N. M., Oberheide, J., Hibbins, R. E., et al. (2021). Tidal variations in the mesosphere and lower thermosphere before, during, and after the 2009 sudden stratospheric warming. *Journal of Geophysical Research*, *126*, e2020JA028827. https://doi.org/10.1029/2020JA028827

Liu, H.-L., & Roble, R. G. (2002). A study of a self-generated stratospheric sudden warming and its mesospheric-lower thermospheric impacts using the coupled TIME-GCM/CCM3. *Journal of Geophysical Research*, *107*(D23), 4695. https://doi.org/10.1029/2001jd001533

Liu, H.-L., Wang, W., Richmond, A. D., & Roble, R. G. (2010). Ionospheric variability due to planetary waves and tides for solar minimum conditions. *Journal of Geophysical Research*, *115*, A00G01. https://doi.org/10.1029/2009ja015188

Matsuno, T. (1971). A dynamical model of the stratospheric sudden warming. *Journal of the Atmospheric Sciences*, *28*, 1479–1494. https://doi.org/10.1175/1520-0469(1971)028<1479:admots>2.0.co;2

McCormack, J. P., Eckermann, S. D., Hoppel, K. W., & Vincent, R. A. (2010). Amplication of the quasi-two day wave through nonlinear interaction with the migrating diurnal tide. *Geophysical Research Letters*, *37*, L16810. https://doi.org/10.1029/2010GL043906

McCormack, J. P., Harvey, V. L., Pedatella, N., Koshin, D., Sato, K., Coy, L., et al. (2021). Intercomparison of middle atmospheric meteorological analyses for the northern hemisphere winter 2009–2010, *Atmospheric Chemistry and Physics*. https://doi.org/10.5194/acp-2021-224

McCormack, J. P., Hoppel, K., Kuhl, D., de Wit, R., Stober, G., Espy, P., et al. (2017). Comparison of mesospheric winds from a high-altitude meteorological analysis system and meteor radar observations during the boreal winters of 2009–2010 and 2012–2013. *Journal of Atmospheric and Solar-Terrestrial Physics*, *154*, 132–166. https://doi.org/10.1016/j.jastp.2016.12.007,2017

McLandress, C. (2002). The seasonal variation of the propagating diurnal tide in the mesosphere and lower thermosphere. Part II: The role of tidal heating and zonal mean winds. *Journal of the Atmospheric Sciences*, *59*, 907–922. https://doi.org/10.1175/1520-0469(2002)059<0907:tsvotp>2.0.co;2

Murphy, D. J., Forbes, J. M., Walterscheid, R. L., Hagan, M. E., Avery, S. K., Aso, T., et al. (2006). A climatology of tides in the Antarctic mesosphere and lower thermosphere. *Journal of Geophysical Research*. https://doi.org/10.1029/2005jd006803

Oberheide, J., Pedatella, N. M., Gan, Q., Kumari, K., Burns, A. G., & Eastes, R. W. (2020). Thermospheric composition O/N response to an altered meridional mean circulation during sudden stratospheric warmings observed by GOLD. *Geophysical Research Letters*, *47*, e2019GL086313. https://doi.org/10.1029/2019gl086313

Pancheva, D., Mukhtarov, P., & Andonov, B. (2009). Nonmigrating tidal activity related to the sudden stratospheric warming in the Arctic winter of 2003/2004. *Annales Geophysicae*, *27*, 975–987. https://doi.org/10.5194/angeo-27-975-2009

Pedatella, N. M., & Forbes, J. M. (2010). Evidence for stratosphere sudden warming-ionosphere coupling due to vertically propagating tides. *Geophysical Research Letters*, *37*, L11104. https://doi.org/10.1029/2010gl043560

Pedatella, N. M., Fuller-Rowell, T., Wang, H., Jin, H., Miyoshi, Y., Fujiwara, H., et al. (2014). The neutral dynamics during the 2009 sudden stratosphere warming simulated by different whole atmosphere models. *Journal of Geophysical Research*, *119*, 1306–1324. https://doi.org/10.1002/2013ja019421

Pedatella, N. M., & Liu, H.-L. (2013). The influence of atmospheric tide and planetary wave variability during sudden stratosphere warmings on the low latitude ionosphere. *Journal of Geophysical Research*, *118*, 5333–5347. https://doi.org/10.1002/jgra.50492

Pedatella, N. M., Liu, H.-L., Marsh, D. R., Raeder, K., Anderson, J. L., Chau, J. L., et al. (2018). Analysis and hindcast experiments of the 2009 sudden stratospheric warming in WACCMX+DART. *Journal of Geophysical Research*, *123*, 3131–3153. https://doi.org/10.1002/2017ja025107

Pedatella, N. M., Liu, H.-L., Richmond, A. D., Maute, A., & Fang, T.-W. (2012). Simulations of solar and lunar tidal variability in the mesosphere and lower thermosphere during sudden stratosphere warmings and their influence on the low-latitude ionosphere. *Journal of Geophysical Research*, *117*, A08326. https://doi.org/10.1029/2012ja017858

Sandford, D. J., Beldon, C. L., Hibbins, R. E., & Mitchell, N. J. (2010). Dynamics of the Antarctic and Arctic mesosphere and lower thermosphere Part1: Mean winds. *Atmospheric Chemistry and Physics*, *10*, 10273–10289. https://doi.org/10.5194/acp-10-10273-2010

Sassi, F., McCormack, J., Tate, J., Kuhl, D., & Baker, N. (2021). Assessing the impact of middle atmosphere observations on day-to-day variability in lower thermospheric winds using WACCM-X. *Journal of Atmospheric and Solar-Terrestrial Physics*, *212*, 105486. https://doi.org/10.1016/j.jastp.2020.105486

Shepherd, M. G., Beagley, S. R., & Fomichev, V. I. (2014). Stratospheric warming influence on the mesosphere/lower thermosphere as seen by the extended CMAM. *Annales Geophysicae*, *32*, 589–608. https://doi.org/10.5194/angeo-32-589-2014

Siddiqui, T. A., Maute, A., & Pedatella, N. (2019). On the importance of interactive ozone chemistry in Earth-system models for studying MLT tidal changes during sudden stratospheric warmings. *Journal of Geophysical Research: Space Physics*, *124*, 10690–10707. https://doi.org/10.1029/2019JA027193

Stober, G., Baumgarten, K., McCormack, J. P., Brown, P., & Czarnecki, J. (2020). Comparative study between ground-based observations and NAVGEM-HA analysis data in the mesosphere and lower thermosphere region. *Atmospheric Chemistry and Physics*, *20*(11), 979–12010. https://doi.org/10.5194/acp-20-11979-2020

Stober, G., Janches, D., Matthias, V., Fritts, D., Marino, J., Moffat-Griffin, T., et al. (2020). Seasonal evolution of winds, atmospheric tides and Reynolds stress components in the Southern hemisphere mesosphere/lower thermosphere in 2019. *Annales Geophysicae* https://doi.org/10.5194/angeo-2020-55

Stober, G., Kuchar, A., Pokhotelov, D., Liu, H., Liu, H.-L., Schmidt, H., et al. (2021). Interhemispheric differences of mesosphere/lower thermosphere winds and tides investigated from three whole atmosphere models and meteor radar observations. *Atmospheric Chemistry and Physics*, *21*(13), 855–13902. https://doi.org/10.5194/acp-21-13855-2021

Teitelbaum, H., & Vial, F. (1991). On tidal variability induced by nonlinear interaction with planetary waves. *Journal of Geophysical Research*, *96*(A8), 14169–14178. https://doi.org/10.1029/91JA01019

Wang, J. C., Palo, S. E., Forbes, J. M., Marino, J., Moffat-Griffin, T., & Mitchell, N. J. (2021). Unusual quasi 10-day planetary wave activity and the ionospheric response during the 2019 Southern Hemisphere sudden stratospheric warming. *Journal of Geophysical Research*, *126*, e2021JA029286. https://doi.org/10.1029/2021JA029286

Wu, D. L., & Eckermann, S. D. (2008). Global gravity wave variances from Aura MLS: Characteristics and interpretation. *Journal of Atmospheric Science*, *65*, 6695–3718. https://doi.org/10.1175/2008JAS2489.1

Yamazaki, Y., Matthias, V., Miyoshi, Y., Stolle, C., Siddiqui, T., Kervalishvili, G., et al. (2020). September 2019 Antarctic sudden stratospheric warming: Quasi-6-day wave burst and ionospheric effects. *Geophysical Research Letters*, *47*, e2019GL086577. https://doi.org/10.1029/2019GL086577

Yu, F. R., Huang, K. M., Zhang, S. D., Huang, C. M., Yi, F., Gong, Y., et al. (2019). Quasi 10- and 16-day wave activities observed through meteor radar and MST radar during stratospheric final warming in 2015 spring. *Journal of Geophysical Research*, *124*, 6040–6056. https://doi.org/10.1029/2019jd030630